Exploration Geophysics, Remote Sensing and Environment XXXI.2 (2024)

DOI: 10.26345/EGRSE-040-24-203

AUTOMATED FAULT DETECTION AND INTERPRETATION USING SEISMIC ATTRIBUTES AND GIS TECHNIQUES: EL FEEL OIL FIELD, MURZUQ BASIN, LIBYA

AUTOMATIZOVANÁ DETEKCE A INTERPRETACE PORUCH POMOCÍ SEISMICKÝCH ATRIBUTŮ A TECHNIK GIS: EL FEEL OIL FIELD, MURZUQ BASIN, LIBYA

Giuma Swei[1], Belgasem Tabib[2], Nureddin Saadi[3], Osama Shtawei[4], Zakariya Farhat[5]

Abstract

This study focuses on the characterization of the subsurface faults and fractures that influence hydrocarbon drilling and production in El Feel field, Murzuq Basin, Libya. The Poor quality of the seismic data posed a significant challenge to the traditional manual fault-detection methods. Two signal processes (AGC and Median filter) were used to enhance the clarity of seismic data. Seismic attributes such as variance, curvature, and ant tracking were used to facilitate faults detection. A GIS-based statistical method was used to interpret and evaluate variances in trends and density of extracted faults in the study area. SRTM (30-m) shaded relief maps were used to investigate the spatial correlation and direction similarity between surface and subsurface structures in the study area. The results of the seismic attribute analysis indicate a moderate degree of faulting and fracturing, with five primary fault patterns. The density maps showed four high-density regions distributed over the entire study area. The approach implemented in this study can improve well placement decision-making, optimize the drilling process and contribute to a more comprehensive understanding of subsurface geological features.

Key words

Seismic attribute, GIS technique, automated fault detection

Introduction

Interpreting faults is an important part of the generation of geological models in any oil and gas field (Zou et al., 2023). However, during drilling operation, faults and fractures are not necessarily desirable, as they may have a pronounced effect on fluid flow patterns, potentially resulting in premature water breakthrough in hydrocarbon reservoirs (Abdullah et al., 2020; Fernandez-Ibanez et al., 2022).

The El Feel oil field in the Murzuq basin has been experiencing the issue of early water breakthroughs in many wells across the field. The interpretation of faults is critical in building a geological model that can guide the development phase in this field. Notably, poor-quality seismic data resulted in difficulties associated with the interpretation of faults and fractured area (Imran et al., 2021).

The 3D seismic data set used in this study was obtained from Mellitah Oil and Gas and consisted of a processed 3D seismic cube in the depth domain. The variance and curvature attributes were used to identify faults (Jaglan et al., 2015; Oliveira, 2023). The ant tracking procedure in Petrel software was also used to locate and track faults through the generated 3D seismic attributes volumes (Kim et al., 2021). Two distinct ant tracking modes were used to identify subsurface faults: (1) passive mode which used to gain a comprehensive understanding of the general subsurface structure and (2) aggressive mode which used to detect minor faults within the targeted area. Preprocess involved preparing the seismic with structural smoothing and filtering, followed by the variance and curvature attributes (El-Farsi and El-shari, 2019).

The interpreted faults were correlated with lineaments determined by shaded relief maps of the Shuttle Radar Topography Mission (SRTM) to investigate the relationship between surface and subsurface structures in the study area (Schowengerdt, 2007).

The GIS-based method was used to analyze and interpret vector results extracted from 3D seismic data. A kernel density algorithm (Silverman, 1986) was used in the calculations of the lineaments density map. A circular search area of 11 km was used and classified into three zones: high, medium and low. The density map at 1 km spatial resolution shows the spread of the faults over the study area. The Line Density was also calculated for each cell in the faults map. The extracted faults were examined by the line density tool of ArcGIS to understand the tectonic relationship of these faults (Meixner et al., 2018).

The results show a moderate number of faults in the study area. Approximately 133 faults in various directions were identified. The dominant trend of extracted faults was observed to be in the NNW-SSE direction. Due to the low quality of the seismic data, it is suggested that the actual number of faults may exceed the number of interpreted faults. Furthermore, the quality of this seismic data is insufficient to accurately identify zones of fracturing. The lineaments density map showed four dense regions in the study area, while blocks of longitudinal parallel faults appear on the line density map. The results can be used to guide the drilling process and enhance well placement decisions with extracted faults network data.

Geological Setting

The Murzuq Basin was formed during the Late Caledonian orogenic phase and underwent two further phases of uplift during the Hercynian (Echickh and Sola 2000). During the Caledonian, the Thambuka and Gargaf Uplifts were emplaced, separating the Murzuq Basin from the Illizi Basin to the west and the Ghadames Basin to the north. The Devonian period saw a renewed uplift of the main

structural units (Davidson et al., 2000). The cumulative tectonic displacements from the Paleozoic, Mesozoic and Cenozoic eras produced the present structural framework of the El Feel field (Echickh and Sola 2000). As a result, there is a wide range of structural styles and fault patterns (Figure 1). The regional lineaments are probably linked to late Precambrian Pan-African fault systems, which largely controlled the early Paleozoic structural evolution and deposition of this field (Echickh and Sola 2000). During the early Paleozoic, there were NW-SE trending linear lows and highs, as evident in the seismic data (Goudarzi, 1967). The current structures are primarily related to Hercynian compressional movements. However, NE-SW trending faults can also be observed which may have formed during a subsequent tectonic event (Davidson et al., 2000). The production in the El Feel field is mainly from the Ordovician Mamunyat formation, which is a significant hydrocarbon reservoir.

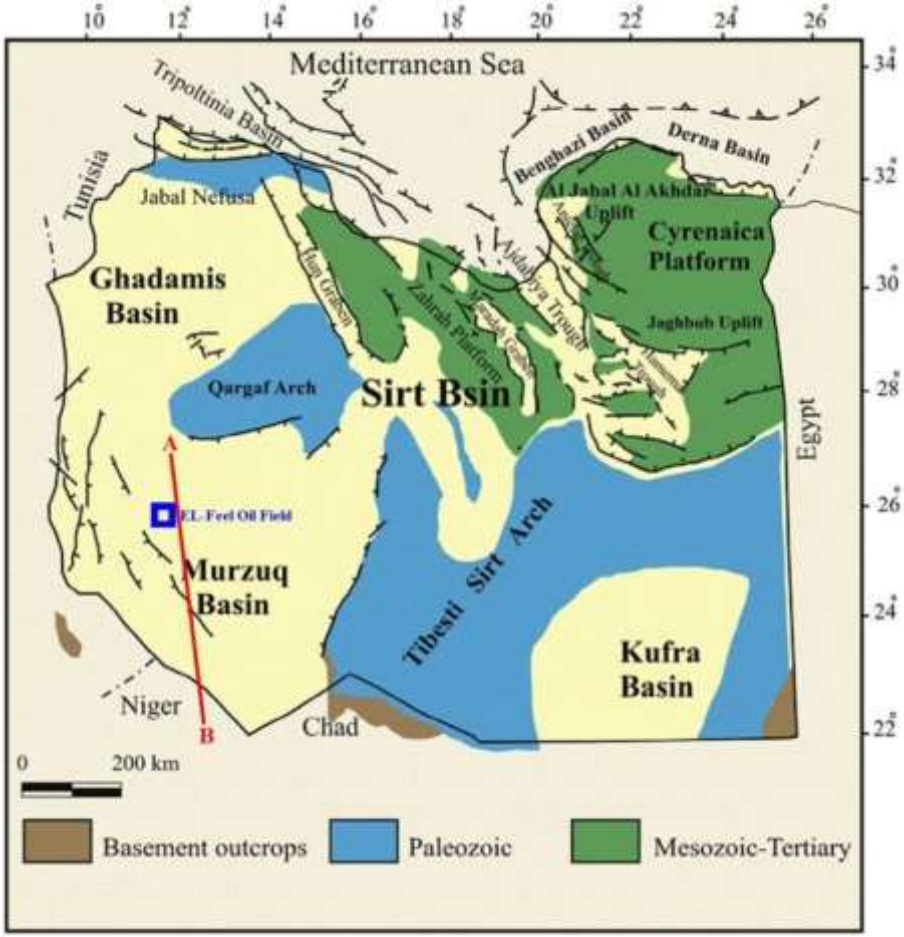

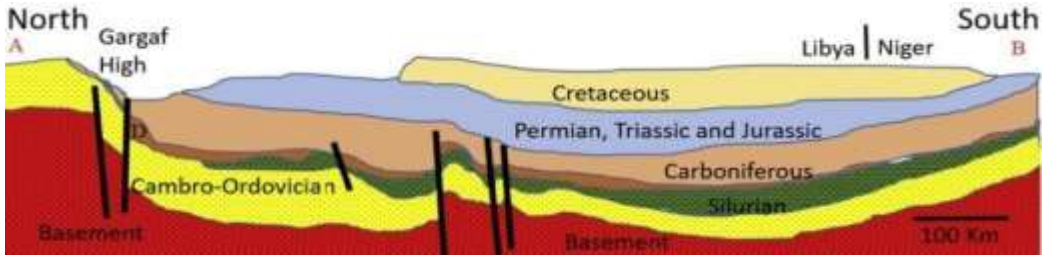

Fig. 1 Tectonic map of Libya including Murzuq Basin (Bellini and Massa, 1980). A north-south cross-section of the Murzuq Basin across the study area (Alansari et al., 2019)

Methodology and Data Analysis

3D Seismic Data

The seismic data obtained initially exhibited suboptimal quality, indicating inherent limitations associated with the seismic acquisition process. In response, enhancement processes were performed on the original seismic cube to improve the data quality. Specifically, two Signal enhancement processes, namely Automatic Gain Control (AGC) and Median filtering, were applied (Liu, 2013; Onajite, 2014).

The AGC process was employed to enhance the seismic data's post-amplitude characteristics and ensure continuity throughout the seismic cube. By equalizing the amplitudes across the seismic volume, the AGC process aimed to improve the overall quality and consistency of the seismic data. The median filter was applied to denoise seismic data and preserve edges. Although the application of these two processes resulted in enhancements to the seismic data, their effectiveness was not optimal to interpret faults on the ordinary seismic. Thus, structural seismic attributes were required to achieve accurate results.

During the creation of ant tracking, a fault detection process was implemented. To prevent the generation of spurious faults in the direction of the seismic survey, a restriction was imposed on the fault detection algorithm. This directional restriction ensured that faults were not erroneously identified in areas aligned with the seismic survey.

The variance attribute (Figure 2) was generated to identify areas of high and low variance in the seismic data, which can be indicative of geological features such as faults, fractures, and stratigraphic changes. In particular, high variance values can indicate areas of faulting or other structural complexity, while low variance values can indicate areas of relatively uniform geology.

Curvature attribute was used to give an insight into the geometry and morphology of subsurface structures. It provides information on the orientation, amplitude, and continuity of seismic reflections and can identify subtle changes in the curvature of subsurface structures that may be indicative of faults. Positive curvature values indicate convex shapes, while negative curvature values indicate concave shapes (Figure 3).

Ant-tracking algorithms were used to analyze seismic attributes to identify and track geologic structures such as faults, fractured zones, and other features. The ant tracking algorithm functions by simulating the behavior of ants and utilizing pheromone trails to locate potential subsurface features. The high-density areas of pheromone trails can then be used to identify potential subsurface structures.

Ant tracking was performed on seismic attributes using the Ant Tracking procedure available in Petrel software. Upon analyzing the variance and curvature attributes, we determined that the variance attribute was the most suitable for generating the ant tracking for this particular seismic data.

For enhancing fault visualization and detection, we used two ant tracking parameters: passive and aggressive. Passive ant tracking is effective in determining the main faults in broad areas (Figure 4). Aggressive ant tracking is effective in determining the minor faults in greater detail compared to the passive ant tracking (Figure 5).

We focused on interpreting faults using different parameters, evaluating their impact on drilling, and production and understanding the structural settings of the study area.

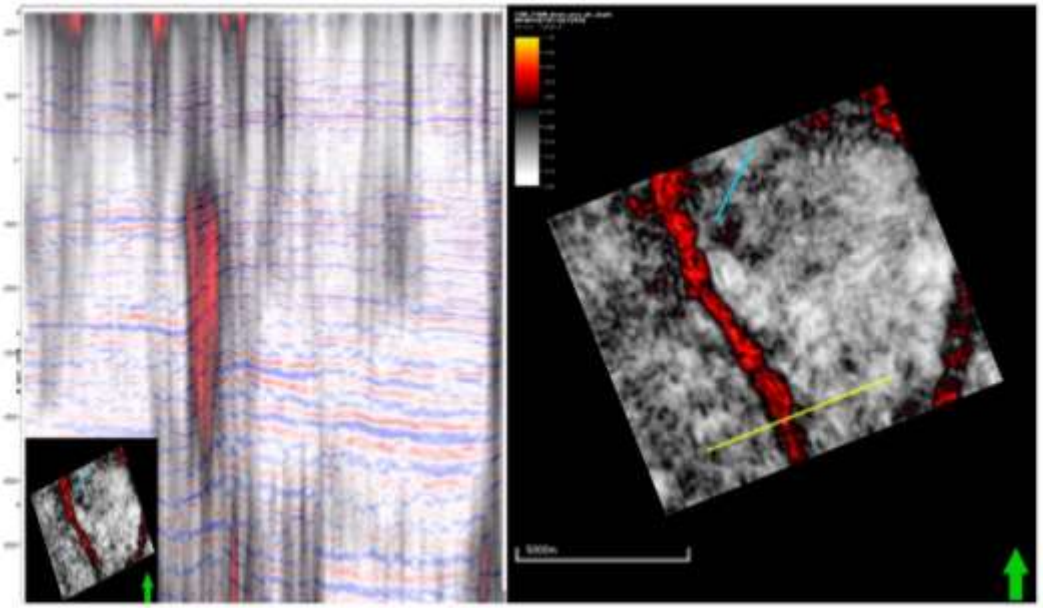

Fig. 2 Variance attribute in section view rendered with the original seismic and depth slice view at the reservoir level

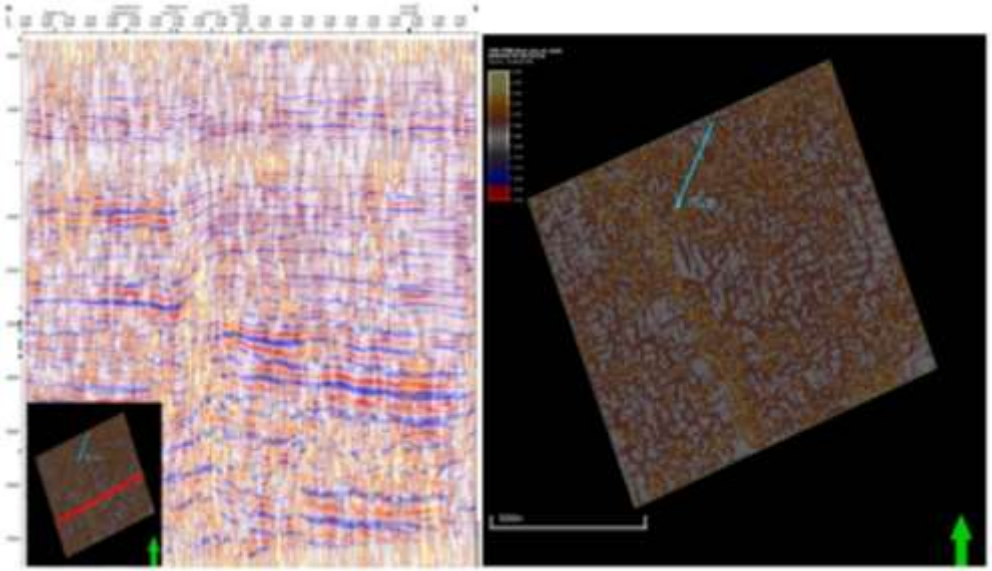

Fig. 3 Curvature attribute in section view rendered with the original seismic

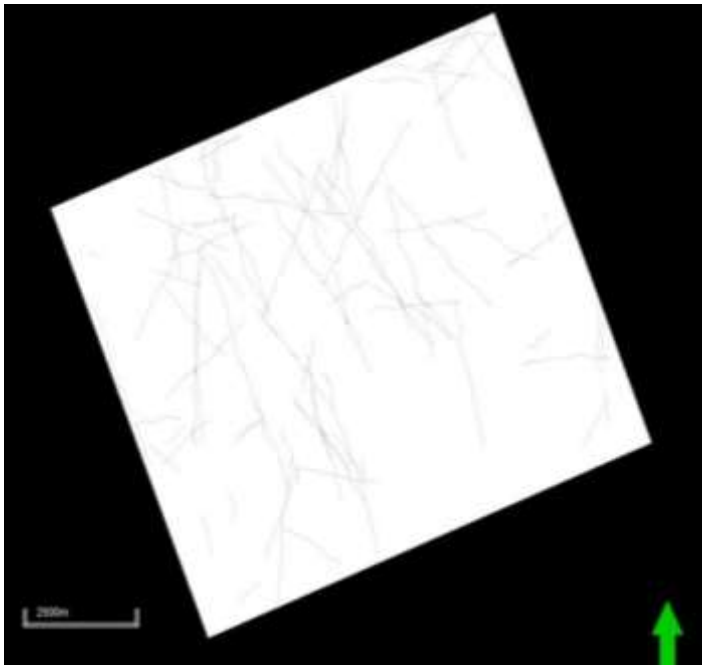

Fig. 4 Ant tracking procedure (passive mode at 914.4 m TVDSS) showing major faults

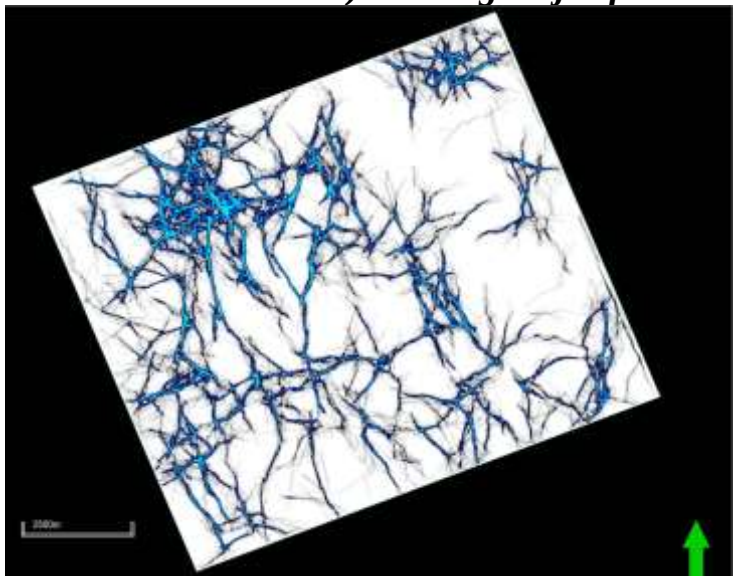

Fig. 5 Ant tracking procedure (aggressive mode) showing small faults

Rose Diagram and Density Maps

All faults interpreted from the ant tracking procedure were imported to ArcGIS as a shapefile. The extracted faults were statistically analyzed to create rose diagrams and to evaluate differences in faults' direction, count, density, and lengths. Thirty major faults were interpreted from the ant tracking procedure (passive mode) (Figure 6). These faults were analyzed and plotted in a rose diagram (Figure 7). The rose diagram shows directions for all fault sets grouped in intervals (10°) such that the length of the tapering bar in each interval is proportional to its frequency distribution (relative proportion). The dominant trends for these faults are NNW-SSE, NW-SE, and NNE-SSW. Figure 8 shows detailed small faults that were interpreted from the ant tracking procedure (aggressive mode). The approximately 133 faults recognized within the site region were statistically analyzed by rose diagram (Figure 9). The prevailing trends in this rose diagram are NNW-SSE, N-S, NNE-SSW, NE-SW, and E-W.

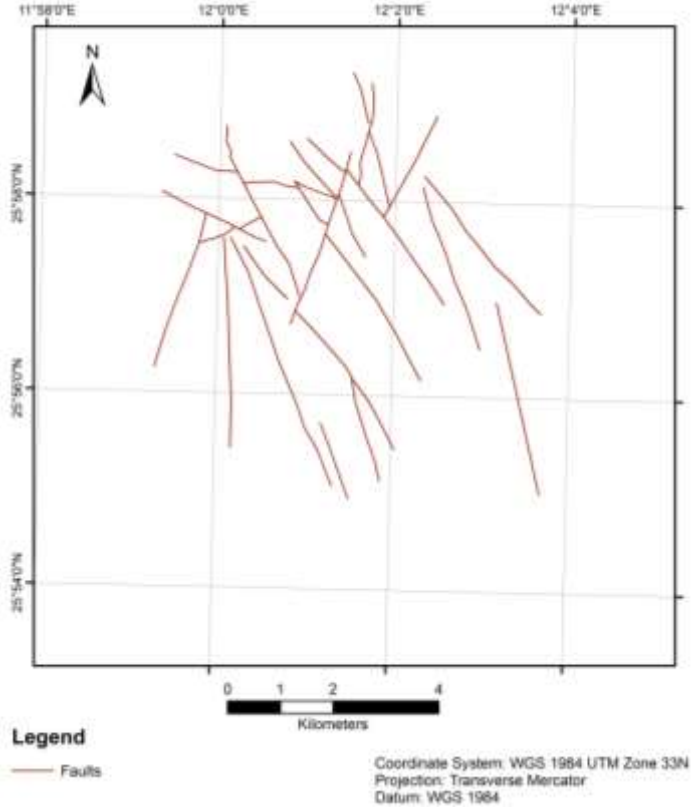

Fig. 6 Major faults interpreted from the ant tracking procedure (passive mode)

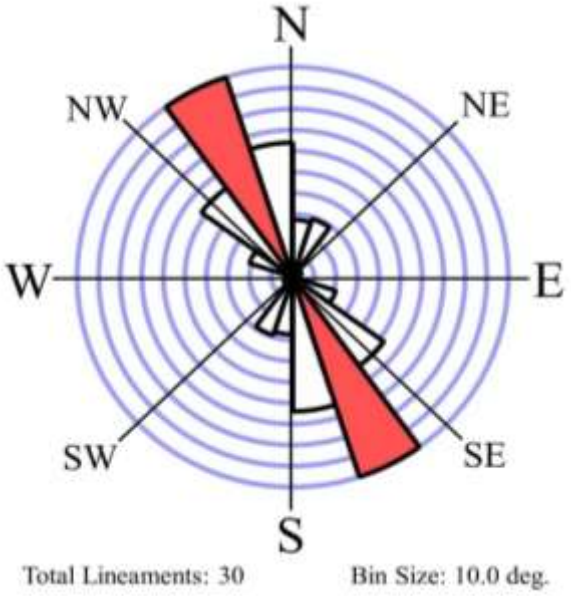

Fig. 7 Rose diagram of faults interpreted from the ant tracking procedure (passive mode). The rose diagram shows three major fault trends (NNW-SSE, NW-SE, and NNE-SSW)

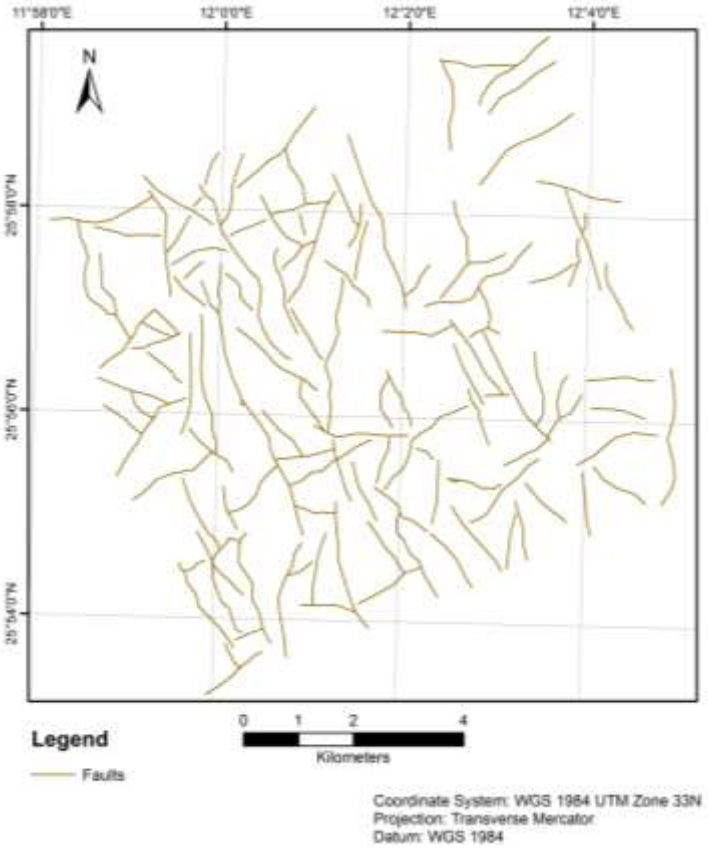

Fig. 8 Detailed small faults interpreted from the ant tracking procedure (aggressive mode)

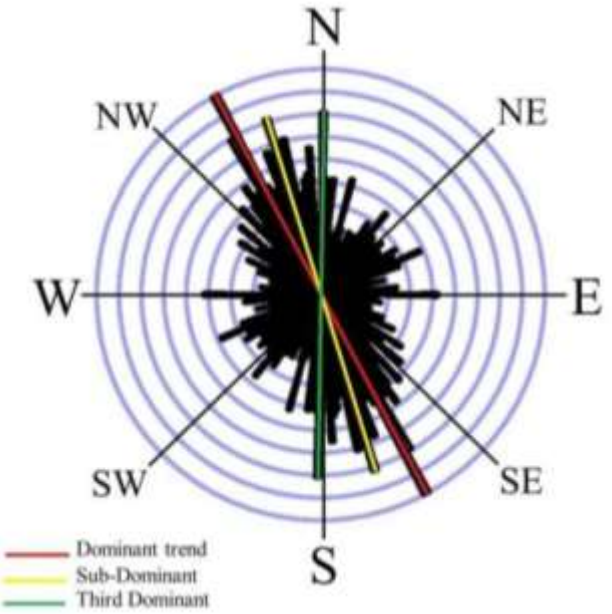

Fig. 9 Rose diagram of faults interpreted from the ant tracking procedure (aggressive mode). The rose diagram shows five major fault trends (NNW-SSE, N-S, NNE-SSW, NE-SW, and E-W)

The Kernel Density tool in ArcGIS was used to calculate a magnitude-per-unit area for the 133 faults that interpreted from the ant tracking procedure (aggressive mode) using a kernel function to fit a smoothly tapered surface to each polyline. For ArcGIS 10.2.1, the default search radius is calculated based on the spatial configuration and the number of input points. Three zones—high, medium, and

low—were employed to a circular search area of 11 km. The generated density map has a resolution of 1 km. High-density faults regions appear in red-orange, medium in yellow, and low in light green and dark green, respectively (Figure 10).

Line density map was generated to help classify these faults by focusing on a single element rather than a region. Figure 11 shows the line density map of the 133 interpreted faults, separated into three density levels: high in red, medium in yellow, and low in green.

Grayscale Shaded Relief Map of SRTM Data

In this study, the SRTM data were used to create shaded relief maps with a z-scale factor of 1. SRTM image reveals the general topographical map of the study area. The shaded relief image is used as a way to make SRTM data appear more three dimensional. With shaded relief, terrain features such as ridges and lineaments appear much more prominent and recognizable.

According to the geological setting of the study area, the prevailing lineaments trend was observed to be in the NW-SE direction. Therefore, sunlight coming from the NE-SW was used to mitigate azimuth biasing effects (Jansson and Glasser, 2005), and enhance the visual detection of linear features in the dominant trend (Soulakellis et al., 2006; Singh et al., 2007). Several azimuth and elevation angles of simulated sun illumination were tested in this study to improve the visual detection of surface faults in the study area. The NE-SW azimuth angle was very useful for enhancing visual detection. A low sun-elevation angle (30º to 40º) was more significant for visual detection of surface faults. Lineaments extracted from the all-sun azimuth directions and elevations were integrated into a single image. The zooming-in facility introduced more flexibility to the visual interpretation and correlation between many linear features in the study area. The extracted lineaments were manually mapped through on-screen digitization process based on tone and texture of shaded relief maps and drainage patterns. The extracted lineaments were statistically analyzed to create rose diagrams and to display trends distribution.

Figure 12 shows the SRTM image revealed buried valleys in the study area. Figure 13 shows an SRTM-DEM Shaded-relief image derived using a light source azimuth of NE-SW and an elevation of 35°. It shows the major extracted lineaments that appeared in the study area. The extracted lineaments were statistically analyzed by rose diagram (Figure 14). The rose diagram revealed three dominant trends: NNW-SSE, NW-SE, and NE-SW.

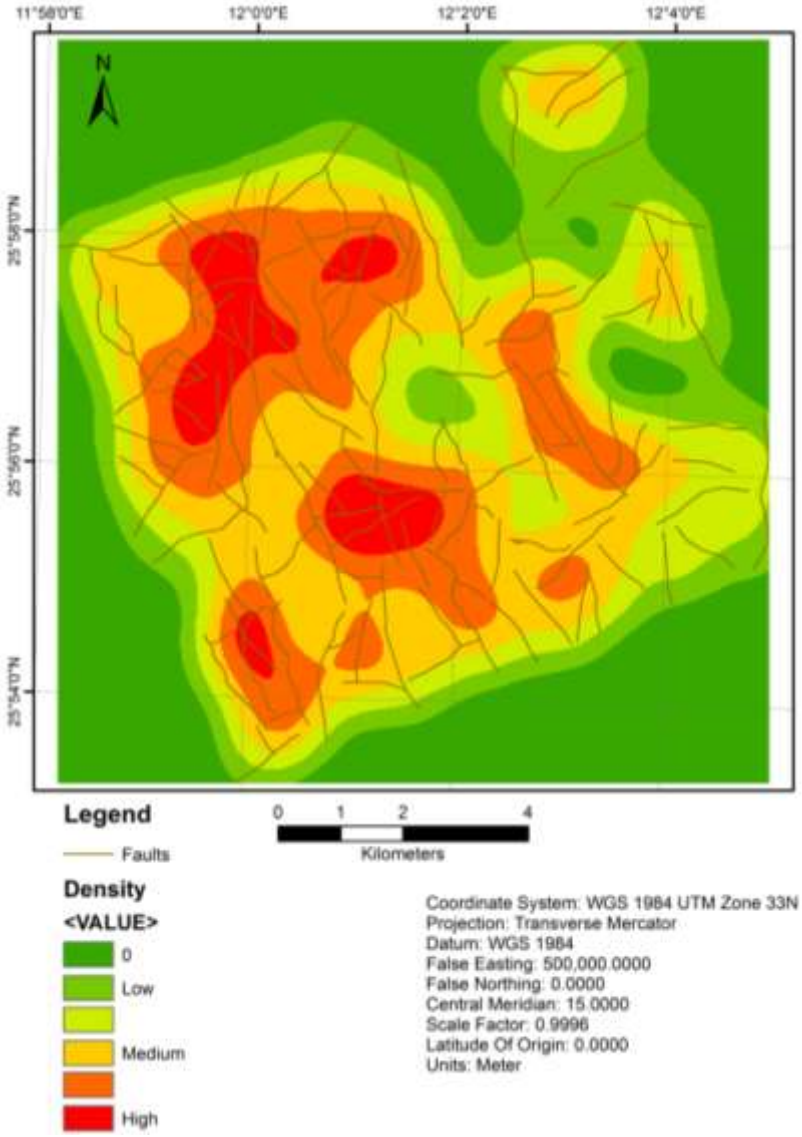

Fig. 10 Density map of the faults interpreted from the ant tracking procedure (aggressive mode). High-density faults regions appear in red-orange, medium in yellow, and low in light green-dark green, respectively

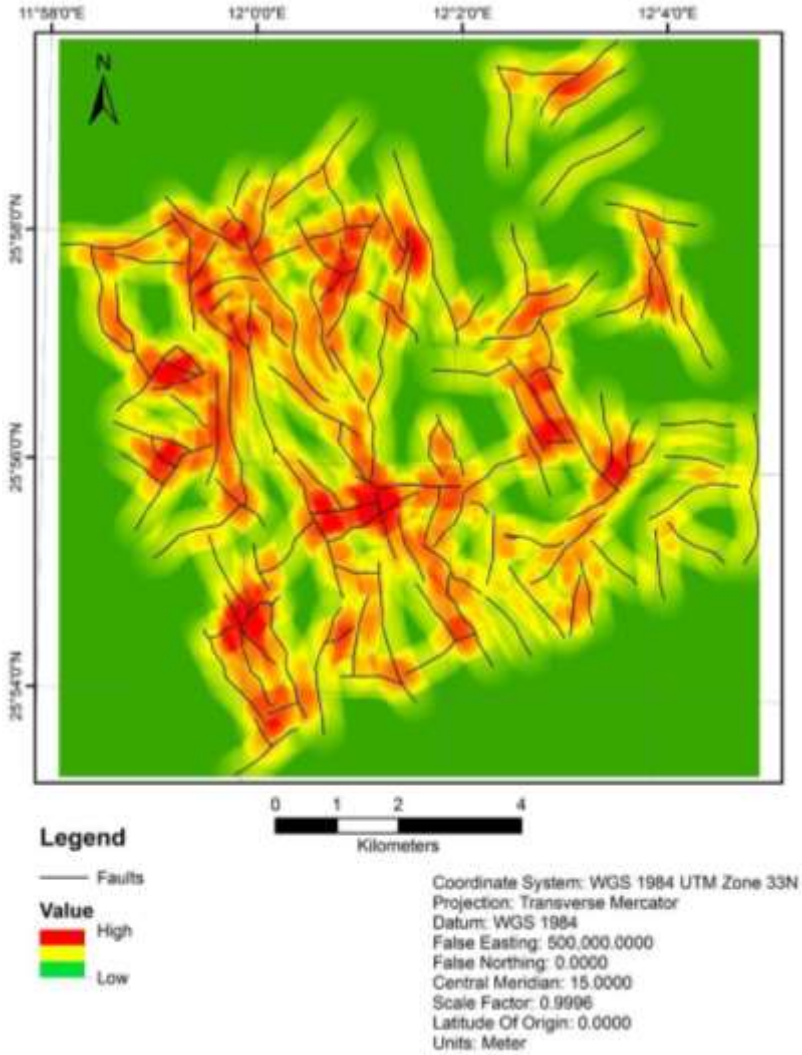

Fig. 11 Line density map of the faults interpreted from the ant tracking procedure (aggressive mode). The map shows four density levels: high in red, medium in yellow, and low in green

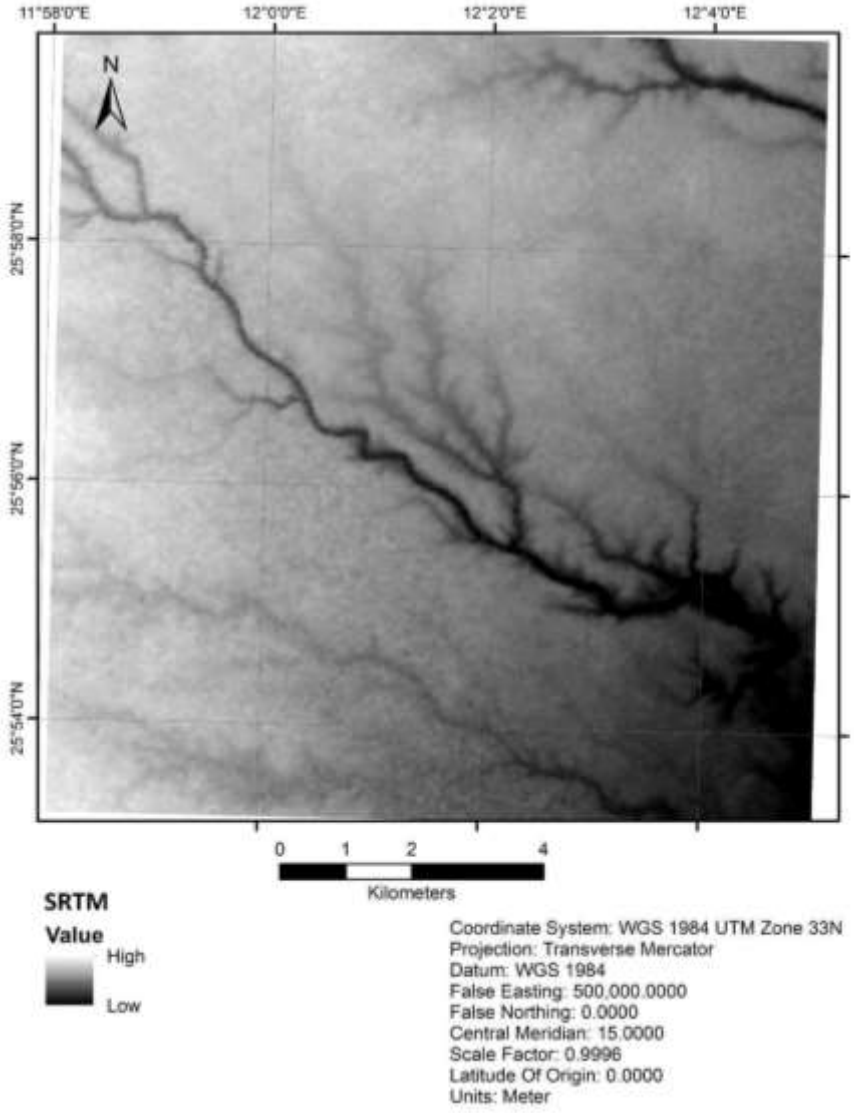

Fig. 12 SRTM image shows the buried valleys in the study area visible as the dark band of lower elevation running diagonally NW-SE

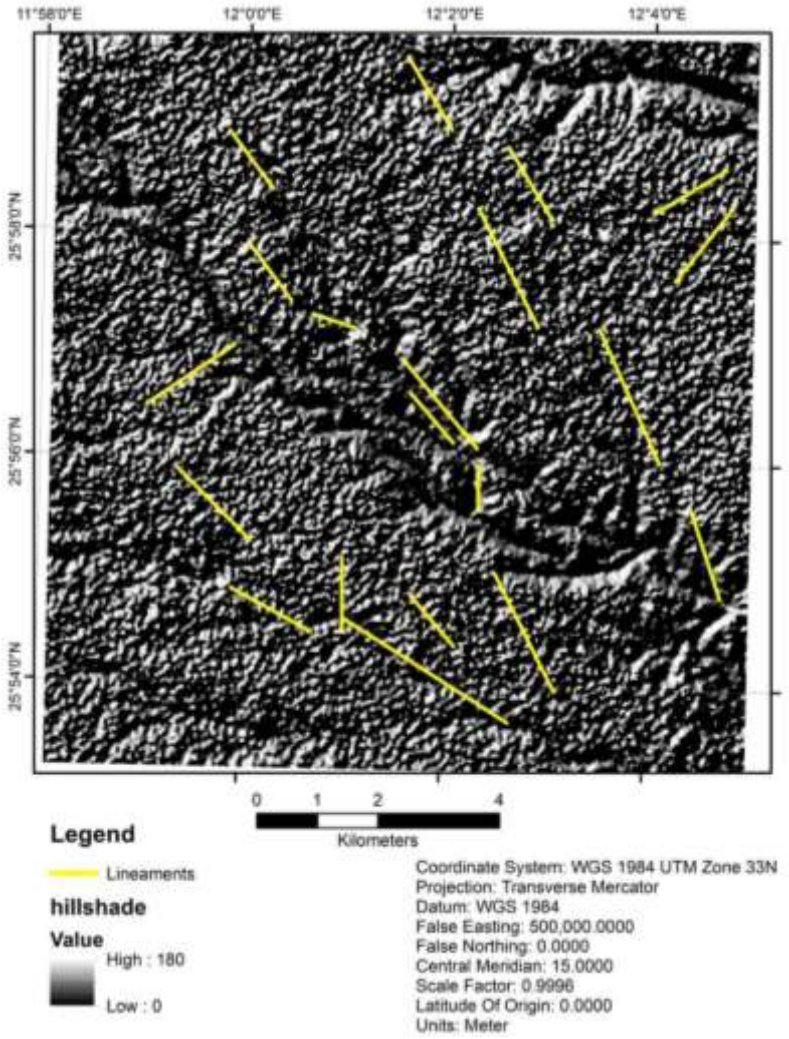

Fig. 13 SRTM-DEM Shaded-relief image derived using a light source azimuth of NE-SW and an elevation of 35°. It is overlaid by lineaments extracted from shaded relief maps

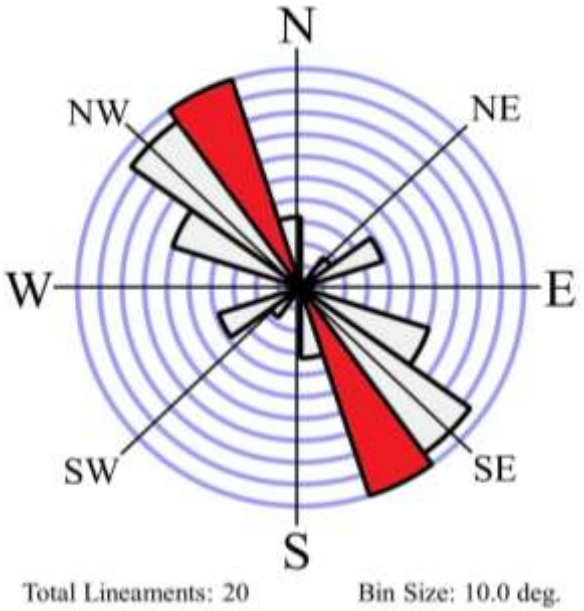

Fig. 14 Rose diagram illustrating surficial lineaments trends extracted from the shaded relief maps. The rose diagram shows three major lineaments trends: NNW-SSE, NW-SE, and NE-SW

Results and Discussion

Through the application of seismic attribute analysis and subsequent interpretation of faults, the area under investigation was successfully delineated in terms of major and minor faults (Figures 4 and 5). The quantity of faults identified by the aggressive mode exceeded those identified by the passive mode. This objective was achieved through the control of parameters during the generation of the ant tracking procedure, which involved a two-level approach: passive and aggressive. Incorporating the ant tracking procedure extracted from variance attribute, a total of 163 faults (133 faults from the aggressive and 30 faults from the passive mode) were successfully interpreted within the study area at different trends (NNW-SSE, NW-SE, NNE-SSW, NE-SW, N-S, and E-W).

Using aggressive ant-tracking, ten faults were interpreted in the area surrounding the proposed well (Figure 15). The faults trended in NNW-SSE, E-W, and NE-SW directions, and were located at varying distances from the wellbore entry point to the reservoir (Table 1).

Tab. 1 The distances between the proposed well and the surrounding faults at the top reservoir level

Fault name	Distance from the entry point (m)
Fault 1 around Z-97-Div	228.00
Fault 2 around Z-97-Div	61.00
Fault 3 around Z-97-Div	176.00
Fault 4 around Z-97-Div	287.00
Fault 5 around Z-97-Div	486.00
Fault 6 around Z-97-Div	573.00
Fault 7 around Z-97-Div	497.00
Fault 8 around Z-97-Div	631.00
Fault 9 around Z-97-Div	355.00
Fault 10 around Z-97-Div	463.00

The density map of the faults shows different patterns. Four high-density regions are distributed over the entire study area, located in the northwest, south, east, and southwest respectively (Figure 10). The dominant trend in the higher-density regions is mainly NNW-SSE to NW-SE, while in the low-density regions the individual faults with random directions mainly appear in the central and northeast regions of the study area.

The longitudinal blocks of parallel faults appearing in the line density map may indicate the existence of local horst and graben blocks inside the study area.

The rose diagram (Figure 9) indicates that two major fault patterns (NNW-SSE and N-S) characterize the investigated area. The analysis indicates that the dominant subsurface faults trend in the NNW-SSE direction, whereas the N-S trend was observed to be subordinate. Other directions with significant representation include NNE-SSW and E-W, while the remaining directions are statistically unimportant. These divergent and different directions may indicate that the Murziq Basin was active at several stages, which probably reactivated the study area several times and introduced different new generations of faulting.

SRTM and shaded relief maps showed lineaments and submerged valleys in an NW direction, which is consistent with the direction of some faults extracted from the ant tracking procedure. This relative agreement between the results of subsurface data and surface data may indicate that the origin of surface lineaments is structural.

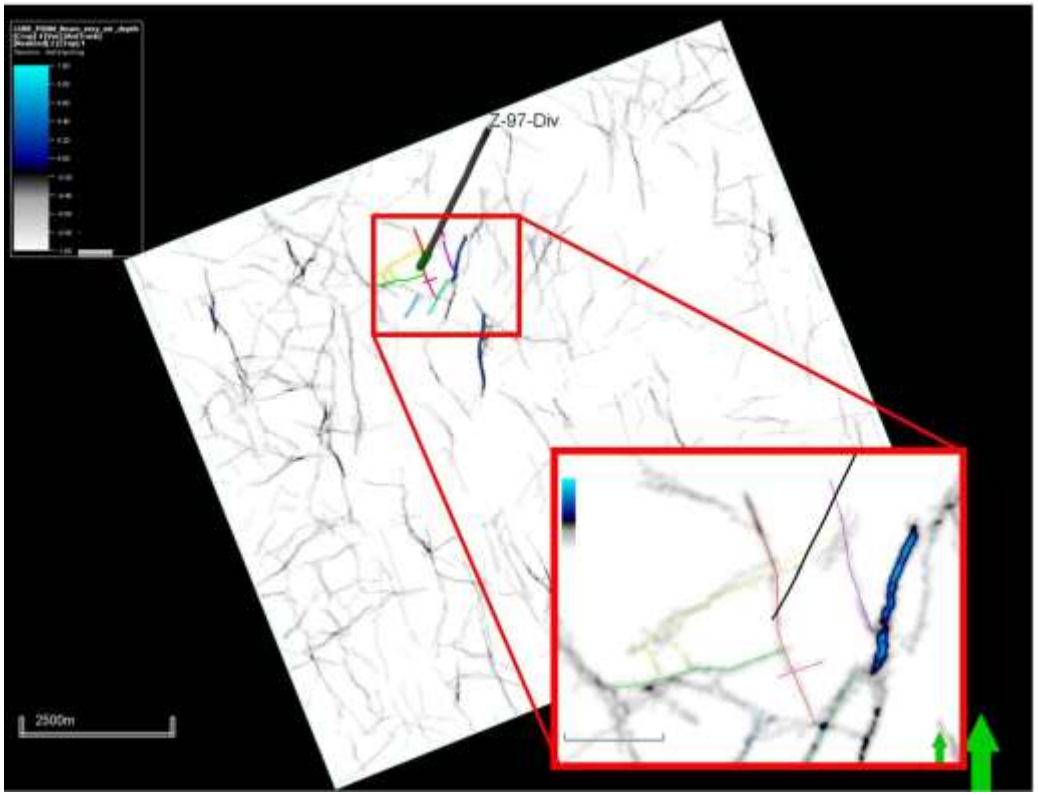

Fig. 15 The interpreted faults around the proposed well (aggressive mode)

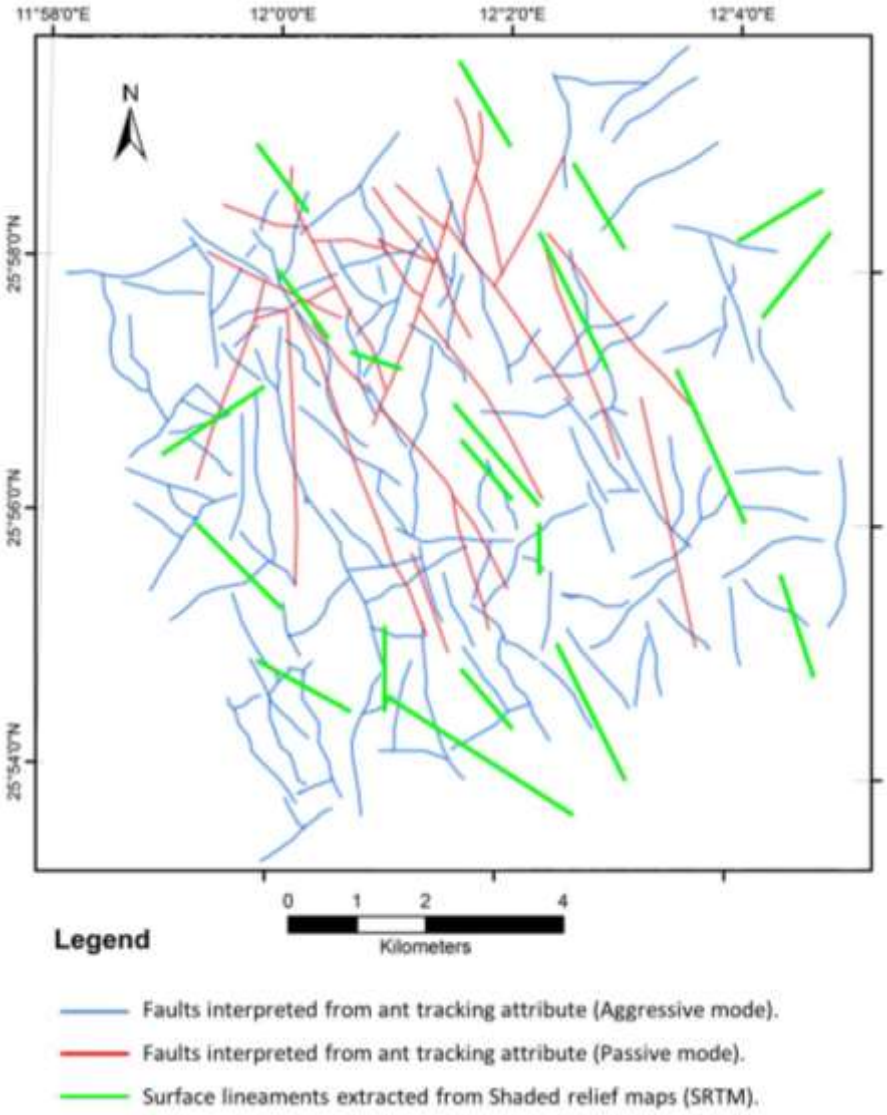

Fig. 16 Faults and lineaments extracted from passive mode, aggressive mode and shade relief maps

Figure 16 is comparing the faults and lineaments extracted from the 3D seismic data and SRTM shaded relief map. The figure shows a match between the subsurface and surface lineaments in the prevailing trend and density. This probably indicates a close tectonic relationship between the surface and subsurface lineaments in the study area. Therefore it is expected to find more Local and regional faults in the same prevailing trend.

The results of this study indicate that the Murzuq Basin was active at several stages and probably affected by many major tectonic episodes. Most of the fault trends revealed by this study (NNW-SSE, N-S, NNE-SSW, NE-SW, and E-W) were recognized by many previous researches and studies on Murzuq Basin.

The Murzuq Basin comprises several different areas with variations in the underlying basement's rheological properties. These basement heterogeneities include several large N, NE, and NW striking structures in the Murzuq and Ghadames basins that were active at different times during the Devonian. Geological maps of the SW margin of the Murzuq basin depict an N-S and NW-SE structural trend in the basement as in the central part of the basin (Adamson, 1999).

Beswetherick (1995, as cited in Adamson, 1999) stated that the variety of structures observed, generally strike N-S and are interpreted to form a regional scale. Also, palaeocurrent data and sedimentological analysis of Palaeozoic sedimentary rocks in North Africa have highlighted a general N or NW inclined continental margin (Clarke-Lowes, 1985; Klitzsch, 1981).

Faults analogous to the N and NE striking, large scale and closely spaced faults observed in the central area of the basin were not observed in outcrop on the west or northern flanks of the basin, and are not reported on the eastern flank. The vast majority of the structures observed on the southern flank of the Gargaf Arch are E-W silicified fault zones (Glover, 1999).

Conclusion

The poor quality of the seismic data has hindered the detection of faults, which caused mud loss during previous drilling operations in the El Feel field. Moreover, these faults and fractures served as pathways for water to enter the wellbore or reservoir.

This study suggests an improved approach for automating the process of detecting and extracting faults and using GIS technology for analyzing and interpreting the results. The results of this study indicate a moderate degree of faulting and fracturing in the study area. The analysis of extracted faults indicates that the study area is characterized by five primary fault patterns (NNW-SSE, N-S, NNE-SSW, NE-SW, and E-W). The density maps showed four high-density regions located in the northwest, south, east, and southwest of the study area.

It is highly recommended to utilize data integration, rose diagrams, and density maps on the field and basin scale to reduce the ambiguity of geological structure and avoid drilling challenges and problems.

Acknowledgements

The authors are grateful to Mellitah Oil & Gas Company for providing the required data for this research work. We would like to thank the Geological & Geophysical Department, Mellitah, and all colleagues for their support and constructive input. The authors are grateful to the editor and anonymous reviewers for helpful remarks and suggestions.

References

ABDULLAH, N., HASAN, N., SAEID, N., MOHYALDINN, M.E., ZAHRAN, E.S.M.M. 2020. The study of the effect of fault transmissibility on the reservoir production using reservoir simulation—Cornea Field, Western Australia, *Journal of Petroleum Exploration and Production Technology* 10, 739-753. DOI: https://doi.org/10.1007/s13202-019-00791-6

ADAMSON, K.R. 1999. *Evolution of the Murzuq Basin, Southwest Libya, and Surrounding Region during the Devonian*. PhD thesis, University of Wales, Aberystwyth, 321 p.

ALANSARI, A., SALIM, A.M., JANJUHAH, H.T., ABD RAHMAN, A.H., FELLO, N.M. 2019. Quantification of clay mineral microporosity and its application to water saturation and effective porosity estimation: A case study from Upper Ordovician Sandstone reservoir, Libya. *Journal of Natural Gas Geoscience* 4(3), 139-150. DOI: https://doi.org/10.1016/j.jnggs.2019.04.005

BELLINI, E., MASSA, D. 1980. A stratigraphic contribution to the Palaeozoic of southern basins of Libya. In: Salem, M.J., Busrewil, M.T., (Eds.). *The Geology of Libya*. Academic Press, London, Vol. I, p. 3-5.

CLARKE-LOWES, D.D. 1985. *Palaeozoic cratonic sedimentation in southwest Libya and Saudi Arabia*, Volume 1 (Libya), PhD thesis, University of London, pp 171.

DAVIDSON, L., BESWETHERICK, S., CRAIG, J., EALES, M., FISHER, A., HIMMALI, A., JHO, J., MEJRAB, B., SMART, J. 2000. The structure, stratigraphy and petroleum geology of the Murzuq Basin, southwest Libya. In *Geological exploration in Murzuq Basin* (eds Sola, M. & Worsley, D.), pp. 295–320. Amsterdam: Elsevier. https://doi.org/10.1016/B978-044450611-5/50016-7

ECHICKH, K., SOLA, M.A. 2000. Geology and hydrocarbon occurrences in the Murzuq Basin, SW Libya. In: M.A. SOLA and D. WORSLEY (Eds), *Geological exploration in Murzuq Basin*. Elsevier, Amsterdam, pp. 175–222. https://doi.org/10.1016/B978-044450611-5/50011-8

EL-FARSI, M.N., EL-SHARI, S. 2019. Utilization of seismic attributes for structural pattern detection In Bualawn, Dor Mansour fields, Western Sirt Basin, Libya. *Journal of Science 9(1):*14-16. https://doi.org/10.37376/ljst.v9i1.2198

FERNANDEZ-IBANEZ, F., NOLTING, A., BREITHAUPT, C.I., DARBY, B., MIMOUN, J., HENARES, S. 2022. The properties of faults in the Brazil pre-salt: A reservoir characterization perspective. *Marine and Petroleum Geology*, 146: 105955. https://doi.org/10.1016/j.marpetgeo.2022.105955

GLOVER, R.T. 1999. *Aspects of Intraplate Deformation in Saharan Cratonic Basins*, PhD thesis, University of Wales.

GOUDARZI, G.H. 1967. Stratigraphic and Tectonic Framework of Libya, *AAPG Bulletin*, vol. 876.

Imran, Q.S., Siddiqui, N.A., Latiff, A.H.A., Bashir, Y., Khan, M., Qureshi, K., Al-Masgari, A.A., Ahmed, N., Jamil, M. 2021. Automated fault detection and extraction under gas chimneys using hybrid discontinuity attributes. *Applied Sciences*, 11(16). https://doi.org/10.3390/app11167218

JAGLAN, H., QAYYUM, F., HÉLÈNE, H. 2015. Unconventional seismic attributes for fracture characterization. *First Break*, 33, 101–109. https://doi.org/10.3997/1365-2397.33.3.79520

JANSSON, K., GLASSER, N. 2005. Using Landsat 7 ETM+ imagery and digital terrain models for mapping glacial lineaments on former ice sheet beds. *International Journal of Remote Sensing*, 26, 3931-3941. https://doi.org/10.1080/01431160500106900

KIM, M., YU, J., KANG, N.-K., KIM, B.-Y. 2021. Improved Workflow for Fault Detection and Extraction Using Seismic Attributes and Orientation Clustering. *Applied Sciences*, 11(18), 8734. https://doi.org/10.3390/app11188734

KLITZSCH, E. 1981. Lower Palaeozoic rocks of Libya, Egypt, and Sudan, In *Lower Palaeozoic of the Middle East, Eastern Africa, and Antarctica* (Ed. by C. H. Holland), John Wiley & Sons Ltd, p 131-163.

LIU, Y.K. 2013. Noise reduction by vector median filtering. *Geophysics*, 78, 79–86. https://doi.org/10.1190/geo2012-0232.1

MEIXNER, J., GRIMMER, J.C., BECKER, A., SCHILL, E., KOHL, T. 2018. Comparison of Different Digital Elevation Models and Satellite Imagery for Lineament Analysis: Implications for Identification and Spatial Arrangement of Fault Zones in Crystalline Basement Rocks of the Southern Black Forest (Germany). *Journal of Structural Geology*, 108, 256–268. https://doi.org/10.1016/j.jsg.2017.11.006

OLIVEIRA NETO, E.R.D., FATAH, T.Y.A., DIAS, R.M., FREIRE, A.F.M., LUPINACCI, W.M., 2023. Curvature analysis and its correlation with faults and fractures in presalt carbonates, Santos Basin, Brazil. *Marine and Petroleum Geology* 158, 106572. https://doi.org/10.1016/j.marpetgeo.2023.106572 .

ONAJITE, E. 2014. *Seismic Data Analysis Techniques in Hydrocarbon Exploration*. Elsevier; Amsterdam, Netherlands.

SCHOWENGERDT, R.A. 2007. *Remote Sensing: Models and Methods for Image Processing*, 3rd edition. Academic Press, London.

SINGH, A. K., PARKASH, B., CHOUDHURY, P. R. 2007. Integrated use of SRM, Landsat ETM+ data and 3D perspective views to identify the tectonic geomorphology of Dehradun Valley, India. *International Journal of Remote Sensing*, 28, 2403–2414. https://doi.org/10.1080/01431160600993397

SOULAKELLIS, N. A., NOVAK, I. D., ZOUROS, N., LOWMAN, P. D., YATES, J. 2006. Fusing Landsat-5/TM imagery and shaded relief maps in tectonic and geomorphic mapping: Lesvos Island, Greece. *Photogrammetric Engineering and Remote Sensing*, 72, 693-700. https://doi.org/10.14358/PERS.72.6.693

ZOU, J., LIU, G., MA, Q., YU, F., MENG, L., TIAN, B. 2023. Analysis of fault characteristics and oil and gas enrichment differences in the No. 2 structural belt, Nanpu Sag, Bohai Bay Basin, East China. *Frontiers in Earth Science* 10: 1057660. https://doi.org/10.3389/feart.2022.1057660

Authors

[1] Giuma Swei - Department of Geological Engineering, Faculty of Engineering, University of Tripoli, Libya

[2] Belgasem Tabib - Department of Geological & Geophysical, Mellitah Oil & Gas B.V., Libya

[3] Nureddin Saadi (Corresponding Author: n.saadi@uot.edu.ly) - Department of Geological Engineering, Faculty of Engineering, University of Tripoli, Libya

[4] Osama Shtawei - Department of Geological & Geophysical, Mellitah Oil & Gas B.V., Libya

[5] Zakariya Farhat - Department of Geological Engineering, Faculty of Engineering, University of Tripoli, Libya